

Refractive index and phase transformation of sapphire under shock pressures up to 210 GPa

Xiuxia Cao, Yuan Wang, Xuhai Li, Liang Xu, Lixin Liu, Yin Yu, Rui Qin, Wenjun Zhu, Shihui Tang, Lin He, Chuanmin Meng, Botao Zhang, and Xusheng Peng

Citation: *Journal of Applied Physics* **121**, 115903 (2017); doi: 10.1063/1.4978746

View online: <http://dx.doi.org/10.1063/1.4978746>

View Table of Contents: <http://aip.scitation.org/toc/jap/121/11>

Published by the *American Institute of Physics*

HPSTAR
366-2017

Articles you may be interested in

[Equation of state of Mo from shock compression experiments on preheated samples](#)

Journal of Applied Physics **121**, 115904115904 (2017); 10.1063/1.4978607

[Loading-path dependent deformation of nanocrystalline Ta under single- and double-shock, and quasi-isentropic compression](#)

Journal of Applied Physics **121**, 115901115901 (2017); 10.1063/1.4978359

[Spall strength of liquid copper and accuracy of the acoustic method](#)

Journal of Applied Physics **121**, 105901105901 (2017); 10.1063/1.4978251

[Optical absorbances of Gd₃Ga₅O₁₂ single crystals under shock compression to 211 GPa](#)

Journal of Applied Physics **121**, 145901145901 (2017); 10.1063/1.4979634

[Elastic-plastic deformation of molybdenum single crystals shocked along \[100\]](#)

Journal of Applied Physics **121**, 045903045903 (2017); 10.1063/1.4974475

[Weak shock loadings induce potential hot spots formation around an intergranular pore](#)

Journal of Applied Physics **121**, 115102115102 (2017); 10.1063/1.4978355

Applied Physics
Reviews

SAVE THE DATE!
3D Bioprinting: Physical and Chemical Processes
May 2–3, 2017 • Winston Salem, NC, USA

Refractive index and phase transformation of sapphire under shock pressures up to 210 GPa

Xiuxia Cao,¹ Yuan Wang,¹ Xuhai Li,¹ Liang Xu,^{1,2} Lixin Liu,¹ Yin Yu,¹ Rui Qin,¹ Wenjun Zhu,¹ Shihui Tang,³ Lin He,^{3,a)} Chuanmin Meng,^{1,a)} Botao Zhang,¹ and Xusheng Peng¹

¹Key Laboratory of Shock Wave and Detonation Physics, Institute of Fluid Physics, Mianyang 621900, China

²Center for High Pressure Science and Technology Advanced Research, Shanghai 201203, China

³College of Physics and Electronic Engineering, Sichuan Normal University, Chengdu 610068, China

(Received 14 January 2017; accepted 4 March 2017; published online 20 March 2017)

Under shock pressures up to 210 GPa, we measured the refractive index of sapphire at a wavelength of 1550 nm by performing plate impact experiments in order to investigate its refractive-index change behaviors and phase transitions along the Hugoniot state. There were two discontinuities in the refractive index at ~ 65 to 92 GPa and ~ 144 to 163 GPa, respectively. Moreover, above the Hugoniot elastic limit, the pressure dependence of the refractive index was divided into three segments, and there were large differences in their pressure-change trends: the refractive index decreased evidently with pressure in the first segment (~ 20 to 65 GPa), remained nearly constant from ~ 92 to ~ 144 GPa in the second segment, and obviously increased with pressure in the last segment (~ 163 to 210 GPa). Our first-principles calculations suggest that the observed discontinuities were closely related to the corundum-Rh₂O₃(II) and Rh₂O₃(II)-CaIrO₃ structural transitions, and the shock-induced vacancy point defects could be one factor causing these great discrepancies in pressure-change trends. This work provides sapphire refractive-index information in a megabar-pressure range and clear evidence of its shock structural transitions. This not only has a great significance for the velocity correction of laser interferometer experiments and the analysis of sapphire high-pressure properties but also indicates a possible approach to explore the shock transitions of transparent materials. *Published by AIP Publishing.*

[<http://dx.doi.org/10.1063/1.4978746>]

I. INTRODUCTION

Sapphire (Al₂O₃ single crystal) is an important material in high-pressure technology^{1–4} and geosciences.^{5,6} Therefore, obtaining knowledge of its physical properties and structural phase transitions under high pressure is of great technical and scientific interest. For instance, laser interferometer measurements in shock-wave high-pressure experiments require an optical window^{1–4} and transparent sapphire crystal is often used as a window material. Understanding the behavior of sapphire's refractive index change under shock compression is crucial for correctly interpreting such measured data.^{7–12} At present, laser interferometer measurements have developed several types of techniques, such as VISAR (Velocity Interferometer System for Any Reflector),^{7–10} PDV (Photon Doppler Velocimetry),¹¹ DPS (Doppler Pin System, which operates at a 1550 nm laser wavelength and is similar to PDV),^{12,13} DISAR (Displacement Interferometer System for Any Reflector),¹⁴ and so on. Because laser wavelengths are set at 532 nm in VISAR and at 1550 nm in DISAR, PDV, and DPS, the refractive-index information of shocked window materials at these wavelengths is essential. However, experimental investigations of the sapphire refractive index have mainly focused on pressures below its Hugoniot elastic limit (HEL)^{7–11} and the refractive index at both 532 nm and

1550 nm showed a monotonously linear variation with pressure. Recently, Cao *et al.* measured the sapphire refractive index at 1550 nm at shock pressures up to 65 GPa and found that, in contrast to the small change below the HEL, the refractive index above the HEL showed an obvious decrease with increasing shock pressure.¹² Even so, information on the sapphire refractive index at higher shock-pressure conditions is still unknown. Whether such information can be obtained by simple extrapolations of existing experimental data is undecided; the structural transitions of sapphire in a pressure range of ~ 80 to 200 GPa have been observed in static high-pressure experiments.^{15–17} If these transitions occur in shocked sapphire, they might have some effect on its refractive-index change behaviors. Therefore, to provide refractive-index data of the sapphire window at a broader shock-pressure range, further experimental study is necessary.

In addition, although static high-pressure experiments have given explicit evidence of corundum-Rh₂O₃ (II) and Rh₂O₃ (II)-CaIrO₃ structural transitions up to 200 GPa,^{15–17} whether they occur in shocked sapphire or not is still unclear. Extensive shock experiments at pressures up to 340 GPa have not indicated evidence of shock transitions in sapphire.^{18–21} On the other hand, experimental studies²² found a sudden increase in electric conductivity in sapphire at a shock pressure of 155 GPa. Although this increase could be attributed to a shock-induced structural transition in sapphire, a clear interpretation for the measured electric conductivity data is

^{a)}Author to whom correspondence should be addressed. Electronic addresses: linhe63@163.com and mcm901570@126.com

complicated and difficult.^{6,23,24} Therefore, seeking other experimental approaches to probe the shock-induced phase transitions in sapphire is of great interest. In diamond anvil cell (DAC) studies, A. Dewaele *et al.* found that careful refractive index measurement could detect phase changes with volume changes as small as 2%.²⁵ In addition, Zhou *et al.* observed that shock-induced phase transitions of a GGG single crystal resulted in different change behaviors of the refractive index with pressure or density.²⁶ This seems to suggest that the refractive-index measurement of shocked sapphire is a possible way to acquire its phase-transition information. If so, it would provide a new method of shock-transition detection in transparent materials.

In this work, we measured the sapphire refractive index at a wavelength of 1550 nm in the shock-pressure range of 54–210 GPa. To better interpret this experimental data, we also calculated the high-pressure refractive indices of sapphire at 1550 nm based on first-principles methods and static high-pressure results. This data allowed us to analyze the physical mechanisms of the refractive-index change and identify if shock-induced phase transitions occur in sapphire.

II. EXPERIMENTAL METHOD

In shock wave experiments, laser interferometer techniques, such as VISAR, DISAR, PDV, and DPS, are widely used to measure the particle velocity of the driver-window interface.^{7–13,26–28} By using these methods, laser light back scattered from the interface is utilized to generate an interferometer fringe signal, whose beat frequency is proportional to the interface particle velocity. However, due to the refractive-index change of the shocked window, the measured interface particle velocity is not the true velocity, but merely an apparent one (u_{APP}), which is related to the window's optical thickness L ^{26,27} and satisfies the following expression:

$$u_{APP} = -\frac{dL}{dt}, \quad (1)$$

where t denotes time. Generally, optical thickness L ^{26,27} satisfies

$$L = \int_{x_0}^h n(x)dx, \quad (2)$$

where x_0 is the position of the driver-window interface, h is that of the window's rear surface, and $n(x)$ denotes the window's refractive index, which depends on the laser wavelength and the window properties.

When a single shock wave propagates in a window, Eq. (2) is simplified as

$$L = n_0(h - x) + n(x - x_0). \quad (3)$$

Here, n_0 and n denote the refractive indices prior to and following the shock front, respectively, and x are the position of the shock front. Therefore, differentiating Eq. (3) with respect to time t yields

$$u_{APP} = n_0D - n(D - u), \quad (4)$$

where

$$D = \frac{dx}{dt} \quad (4a)$$

and

$$u = \frac{dx_0}{dt}. \quad (4b)$$

Here, D and u denote the shock velocity and the true particle velocity of the shock-compressed window, respectively. Eq. (4) also shows that

$$n = \frac{u_{APP} - n_0D}{u - D}. \quad (5)$$

For an elastic-plastic two-wave structure within an optical window, Eq. (2) becomes

$$L = n_0(h - x_E) + n_E(x_E - x_P) + n_P(x_P - x_0). \quad (6)$$

Here, subscripts E and P refer to the elastic and plastic wave, respectively. To differentiate, Eq. (6) gives

$$u_{APP,P} = n_0D_E - n_E(D_E - D_P) - n_P(D_P - u_P). \quad (7)$$

According to Eq. (7), the refractive index following the plastic wave front can be expressed as

$$n_P = \frac{u_{APP,P} - n_0D_P + (n_E - n_0)(D_E - D_P)}{u_P - D_P}. \quad (8)$$

Equations (5) and (8) have been widely used in the refractive index measurement of transparent materials under shock compression.^{12,13,26,28} In these measurements, the parameters u_{APP} and D were directly measured by laser interferometers. The true particle velocity u was calculated by the impedance match method or other methods. Based on this theory, we designed two different target set-ups to measure the refractive index data of shocked sapphire at 1550 nm, as shown in Fig. 1. For an elastic-plastic two-wave structure within sapphire samples, a diagram of the target configuration is illustrated in Fig. 1(a). The driver was backed by two sample disks that were fixed together and ~ 600 nm Cu films were fully and partly ($\Phi 5$ mm) deposited on the front face of both samples, respectively. A three-channel DPS was used to measure the movement of the driver-sample and sample-sample interface velocity, respectively. Fig. 1(b) presents the target configuration of the single-wave structure. A sample disk was mounted behind the driver plate and ~ 600 nm Cu film was fully deposited on the sample disk surface to reflect the probe laser light. In addition, a single-channel DPS was used to measure the particle velocity histories of the driver-sample interface and the sample's free surface.

$\Phi 25 \times 3$ mm or $\Phi 25 \times 4$ mm sapphire single crystals were used as experimental samples and cut into cylindrical disks with bottom surfaces parallel to the r -planes. Metallic flyers were launched on a two-stage light gas gun to impact the driver-sample targets, and the impact velocities were measured by a magnetic velocimetry system. All optical signals were recorded in an oscilloscope with a sample rate of

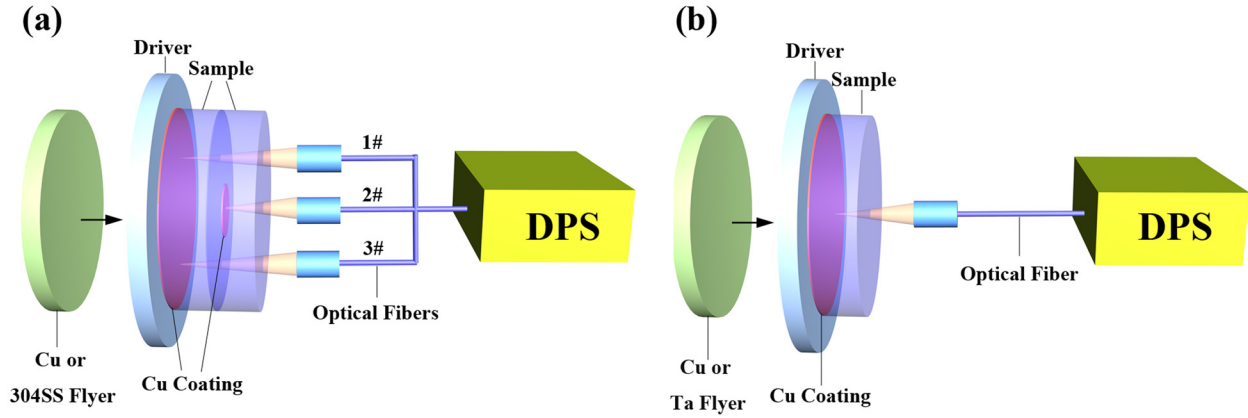


FIG. 1. Diagram of the experimental set-up for the (a) elastic-plastic wave and (b) single wave zone.

40 GSa/s and bandwidth of 13 GHz and analyzed using a short-time Fourier transform method (the FFT length, window length, and overlap parameters were 2024, 256, and 128, respectively) to extract the particle velocity profile. The related experimental parameters are shown in Table I.

Fig. 2(a) shows the typical particle velocity histories measured from the elastic-plastic two-wave structure zone (shot A02). The noise in the velocity data might be related to the shock-induced heterogeneous deformations in the sapphire single crystal as well as the deterioration of its optical transparency. When the shock wave arrived at the driver-sample interface, the apparent particle velocities from DPS-1# and DPS-3# jumped to a value of ~ 4.287 km/s at times t_A and t_B , separately. The ~ 43 ns delay of time t_B after time t_A was due to the tilt of the flyer. As the shock wave continued, an obvious two-wave structure was detected by DPS-2# at the sample-sample interface (after time t_C) and the sample free surface (after time t_E). According to the velocity profiles shown in Fig. 2(a), the shock velocities of both the elastic precursor (D_E) and plastic wave (D_P) were obtained by dividing the sample thickness by the shock transit time of the elastic and plastic waves, respectively. The true particle velocity of the elastic wave u_E equals $u_{FSE}/2$, where u_{FSE} denotes the particle velocity of the elastic wave on the free surface of the sapphire sample. By using an impedance matching method, the true particle velocity of the plastic wave u_P was calculated using the known impact velocity, the shock velocities, and the Hugoniot relation of the driver

plate.^{29,30} Thus, we finally obtained the refractive index values following the elastic and plastic wave front, n_E and n_P , by combining Eqs. (5) and (8).

A typical result from the single-wave structure zone (shot A05) is plotted in Fig. 2(b). Upon the shock wave entering the sample at time t_1 , the apparent particle velocity of the driver-sample interface (u_{APP}) increased sharply to a steady plateau and was followed by another particle-velocity plateau when the shock broke out at time t_2 . Therefore, the shock velocity D was obtained from the sample thickness and the shock transit time ($t_2 - t_1$). After the determination of the true particle velocity u via impedance matching, the refractive index in compression, n , was calculated using Eq. (5). Note that the optical transparency of sapphire deteriorates under megabar shock pressures^{31,32} and the loss of partial apparent particle velocity information was observed when the shock pressure reached above 190 GPa [see Fig. 2(c)]. However, the values of u_{APP} and D can still be clearly determined from the particle velocities shown in Fig. 2(c), which allowed us to obtain the value of the refractive index n .

Given that the apparent particle velocity of the driver-window interface should be constant, we approximated the apparent velocity as the statistical average value of the measured apparent velocities' history profile; its uncertainties are the standard deviation ($<1.7\%$). The transit times were obtained by judging the sudden change in the raw beat frequency data. Uncertainties in this time determination method were assumed to be about 1/2 the time of a single period of the raw frequency data. Finally, the measurement uncertainties of the shock velocity, true velocity, shock pressure, and refractive index of the shocked sample were analyzed with the uncertainty propagation formula, as shown in Table II.

TABLE I. Related materials parameters for shock experiments. The relative uncertainties of the thickness measurements are less than 0.1%.

Shot no.	Flyer/driver materials	Flyer/driver thickness (mm)	Sample thickness (mm)
A01	Cu/Cu	3.519/0.020	4.020/3.006
A02	304SS/304SS	5.475/1.495	4.038/3.009
A03	304SS/304SS	5.079/1.488	4.022/3.030
A04	Cu/Cu	3.488/1.972	3.008
A05	Cu/Cu	3.512/1.989	3.008
A06	304SS/304SS	5.5/1.480	4.013
A07	Ta/Ta	2.040/1.128	3.009
A08	Ta/Ta	1.661/0.988	3.012

III. RESULTS AND DISCUSSION

The experimental results from eight shots in the specimen pressure range of 54–210 GPa are summarized in Table II. Fig. 3 illustrates the measured D - u data together with previous results.^{12,18–21} Overall, our D - u data agree well with those reported in the literature, and a linear relationship can describe the whole D - u data of the plastic wave

$$D = 8.729 (\pm 0.060) + 0.965 (\pm 0.021) u. \quad (9)$$

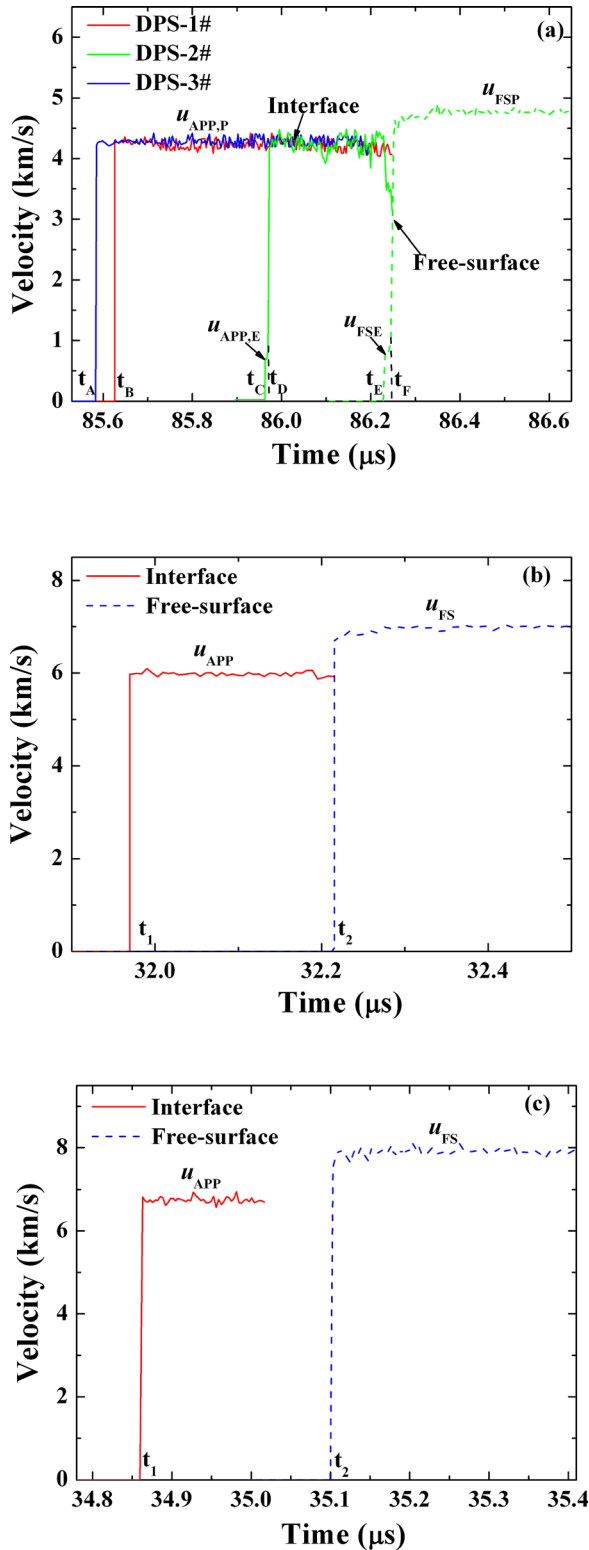


FIG. 2. Typical particle velocity profiles from (a) shot A02, (b) shot A05, and (c) shot A07.

Moreover, the measured volume also changed continuously with pressure in the whole shock compression curve (see Fig. 4), and no sudden changes in volume were observed at the possible phase boundaries that were plotted based on the static pressure data.^{15–17} This means that it is difficult to resolve the shock phase transformations of sapphire with a conventional Hugoniot measurement alone.

In this case, an analysis on measured shock refractive-index data is worthwhile.

The measured refractive index data of sapphire under shock compression are plotted in Figs. 5(a) and 5(b). It is obvious that our refractive-index data in the low-pressure region are consistent with previous results,^{11,12} indicating that our experimental data are highly reliable. Near ~ 20 GPa (the HEL of sapphire), there is an inflexion in the refractive index-density (or pressure) curve. This inflexion behavior is attributed to the transition from elastic to plastic deformation.¹² More interestingly, another two discontinuous phenomena in the refractive index were observed with increasing density or pressure, as shown in Figs. 5(a) and 5(b). The density (or pressure) dependence of the refractive-index above the HEL were divided into three segments: the refractive index decreased evidently with density (or pressure) in the first segment (~ 4.20 to 4.68 g/cm³, ~ 20 to 65 GPa), remained nearly constant in the second segment (~ 4.98 to 5.32 g/cm³, ~ 92 to 144 GPa), and exhibited an obvious increase with density (or pressure) in the last segment (~ 5.48 to 5.84 g/cm³, ~ 163 to 210 GPa). Linear fits of the refractive index as a function of density to the three segments give

$$n = 2.0477 - 0.0726\rho, \quad \text{for } 4.20 < \rho < 4.68 \text{ g/cm}^3, \quad (10)$$

$$n = 1.7185 - 0.0004\rho, \quad \text{for } 4.98 < \rho < 5.32 \text{ g/cm}^3, \quad (11)$$

and

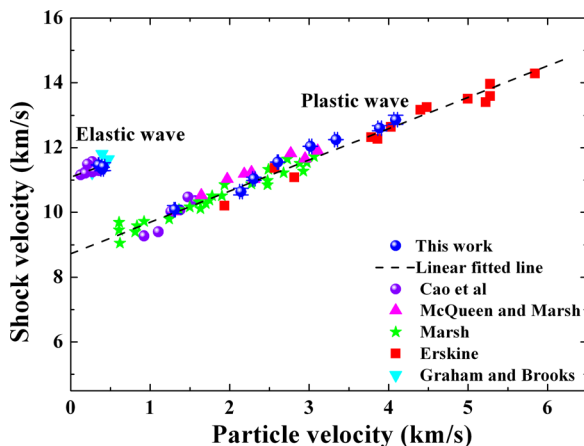
$$n = 1.2025 + 0.0958\rho, \quad \text{for } 5.48 < \rho < 5.84 \text{ g/cm}^3. \quad (12)$$

Note that the errors in the experimental data cannot account for the observed discontinuities (see Figs. 5(a) and 5(b)). Shock-induced defects and temperatures should not be factors causing these phenomena either, although they could affect the refractive index of transparent materials (e.g., a study suggested that shock-induced vacancy point-defects and temperatures may lead to the changes in the LiF refractive-index, but its refractive-index measurements in the wide shock-pressure ranges did not indicate discontinuous behaviors^{11,33}). How to understand these discontinuous phenomena observed in shock refractive-index experiments of sapphire is an intriguing issue. Static high-pressure experiments and theoretical calculations^{6,15–17} have shown that there are two successive high-pressure structural transitions in Al₂O₃ up to 200 GPa, and the pressure and temperature conditions of the two observed refractive-index discontinuities are basically compatible with those of the two high-pressure structural transitions (see Fig. 5). This means that the discontinuous phenomena observed in shock refractive-index measurements of Al₂O₃ could be related to its phase transitions and results from refractive-index measurements in shocked GGG single crystal also support this inference.²⁶ Even so, whether this conjecture is true or not needs to be further investigated. Therefore, we performed first-principles calculations of the high-pressure refractive index of Al₂O₃, based on its phase diagram from static high-pressure experiments and theoretical calculations in the Refs. 6 and 16 (see [supplementary material](#) for more calculation details).

TABLE II. Experimental results. The relative error in the flyer velocity was 0.5%–1%.

Shot No.	Shock wave	Flyer velocity (km/s)	Shock velocity (km/s)	Apparent particle velocity (km/s)	True particle velocity (km/s)	Shock pressure (GPa)	Refractive index
A01	Elastic	2.40	11.46 ± 0.01	0.65 ± 0.01	0.35 ± 0.01	16.0 ± 0.1	1.7426 ± 0.0027
	plastic		10.08 ± 0.13	2.52 ± 0.04	1.31 ± 0.01	54.4 ± 0.6	1.7197 ± 0.0050
A02	Elastic	4.08	11.34 ± 0.05	0.69 ± 0.01	0.40 ± 0.02	17.9 ± 0.7	1.7458 ± 0.0026
	plastic		11.03 ± 0.05	4.29 ± 0.06	2.30 ± 0.02	101.8 ± 1.4	1.7160 ± 0.0073
A03	Elastic	3.79	11.41 ± 0.12	0.74 ± 0.01	0.41 ± 0.02	18.7 ± 0.8	1.7442 ± 0.0029
	plastic		10.64 ± 0.10	3.98 ± 0.05	2.14 ± 0.02	91.9 ± 1.6	1.7177 ± 0.0064
A04	Plastic	5.24	12.04 ± 0.01	5.53 ± 0.06	3.02 ± 0.02	144.8 ± 0.8	1.7175 ± 0.0075
A05	Plastic	5.75	12.25 ± 0.01	5.99 ± 0.06	3.34 ± 0.02	163.0 ± 0.9	1.7282 ± 0.0073
A06	Plastic	4.61	11.55 ± 0.01	4.82 ± 0.03	2.61 ± 0.01	120.0 ± 0.3	1.7161 ± 0.0034
A07	Plastic	5.89	12.60 ± 0.08	6.73 ± 0.09	3.89 ± 0.02	195.3 ± 1.6	1.7521 ± 0.0116
A08	Plastic	6.19	12.86 ± 0.14	6.96 ± 0.11	4.09 ± 0.02	209.7 ± 2.6	1.7662 ± 0.0138

Initially, we obtained the calculated refractive-index data of an Al_2O_3 perfect crystal at 300 K at high pressure (see Fig. 6). Note that the inflexion behavior observed experimentally at ~ 20 GPa does not appear in our calculated results [see an inset in Fig. 6(a)]. This could be because hydrostatic-pressure conditions are adopted in our first-principles calculations.³⁴ Even so, we found that the Corundum- $\text{Rh}_2\text{O}_3(\text{II})$ and $\text{Rh}_2\text{O}_3(\text{II})$ - CaIrO_3 structural transitions did indeed cause an increase in the refractive index, respectively. Moreover, the calculated refractive index in the corundum-phase region decreased obviously with pressure, similar to the change tendency of the experimental data in the first segment [see Fig. 6(a)]. However, the pressure-change tendencies of the calculated refractive-index data points in the $\text{Rh}_2\text{O}_3(\text{II})$ and CaIrO_3 phase regions were different from those of the second and third segments determined by our shock experiments (see Fig. 5(b) and Fig. 6(a)). Shock compression involves the dynamic generation of high temperature and high pressure in the material by high-velocity plate impact and the shock temperature increases with increasing shock pressure. Since shock-induced temperatures in Al_2O_3 may cause an increase of its refractive-index (and the higher temperature due to the larger shock pressure yields a further increase in the refractive-index),³⁵ it seems that shock-induced temperatures could account for the differences between our experimental and calculated results. The temperature dependence of the

FIG. 3. Shock velocity (D) vs. true particle velocity (u).

Al_2O_3 refractive-index at high pressure is unavailable at present, but the temperature dependence at ambient pressure may be used to estimate the effect of temperature on the Al_2O_3 refractive-index at high pressure.³⁵ However, the temperature coefficient of the sapphire refractive-index is very small (by an order of magnitude of $\sim 10^{-5}$ to 10^{-6} K^{-1}), which suggests that the effect of temperature is not enough to account entirely for these differences. A comparison between the calculated and experimental data in the pressure range of ~ 36 to 65 GPa indicated a weak change of the temperature coefficient at high pressure. Here, we attempt to interpret the differences further using shock-induced vacancy point defects for the following reasons: (1) experimental studies have indicated that strong shock compression induces high-concentration point defects in material;³⁶ (2) theoretical calculations show that shock-induced vacancy point defects may obviously influence the refractive index of window materials.³⁷ Interestingly, an investigation of LiF also showed that the calculated refractive-index data in the low shock-pressure

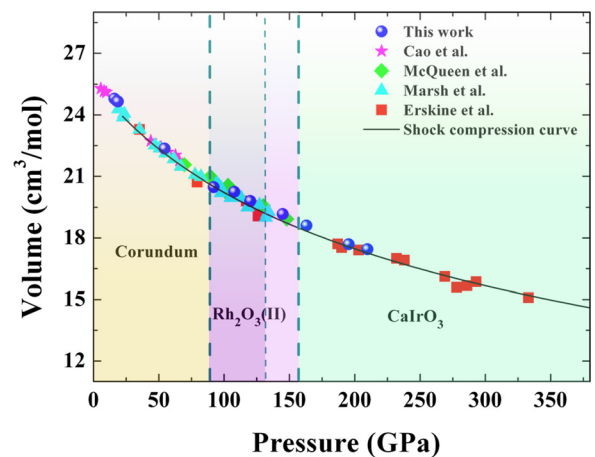


FIG. 4. Volume shown as function of pressure. Solid symbols are the measured data of sapphire under shock compression.^{12,18–20} The solid line is the shock compression curve calculated by applying the Rankine-Hugoniot equations [$v = m(D - u)/(D\rho_0)$, $P = \rho_0 Du$, m , and ρ_0 are the mole mass and density of sapphire under the ambient conditions, respectively] to the Hugoniot data. The thick dashed lines denote the possible corundum- $\text{Rh}_2\text{O}_3(\text{II})$ and $\text{Rh}_2\text{O}_3(\text{II})$ - CaIrO_3 phase boundaries of shocked sapphire, which are plotted based on the static pressure data in Refs. 15 and 17. The thin dashed line is another possible $\text{Rh}_2\text{O}_3(\text{II})$ - CaIrO_3 phase boundary according to the static pressure data in Ref. 16.

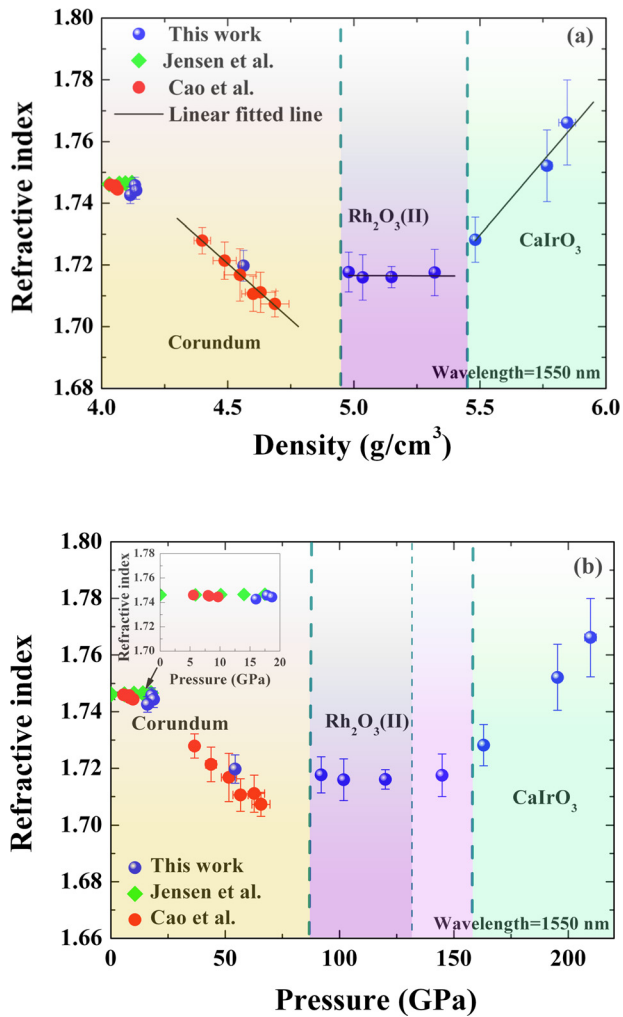


FIG. 5. The measured refractive index is shown as function of (a) shock density and (b) pressure. The dashed lines denote the possible phase boundaries of shocked sapphire based on the static pressure data.^{15–17}

region were consistent with those determined by experiments. However, in the high shock-pressure region, there were obvious discrepancies between them, and it was suggested that these discrepancies could be related to shock-induced vacancy point defects.³⁷ This means that an investigation of the effects of vacancy point defects on the sapphire refractive index in the high-pressure region is worthwhile. Here, we selected three pressure points in the high-pressure region (100 GPa, 131.2 GPa, and 172 GPa) to implement vacancy-defect calculations. The defect concentration increases with shock pressure,³⁶ and first-principles studies of LiF also show that the vacancy-defect concentrations should increase with increasing shock-pressure.³⁷ This shows that models with three different vacancy-defect concentrations are required for three pressure-point vacancy-defect calculations. However, detailed information on the vacancy-defect concentration in sapphire in a shock state is unclear; thus, we can only qualitatively simulate the behavior. Due to our computing resource limitations, we adopted three feasible supercells with 40, 60, and 80 atoms (corresponding to different pressure points) in our vacancy-defect calculations. In these supercells, an Al or O atom is removed to generate an Al or O vacancy, leading to 2.5%, 1.67%, and 1.25% vacancy concentrations, respectively. The

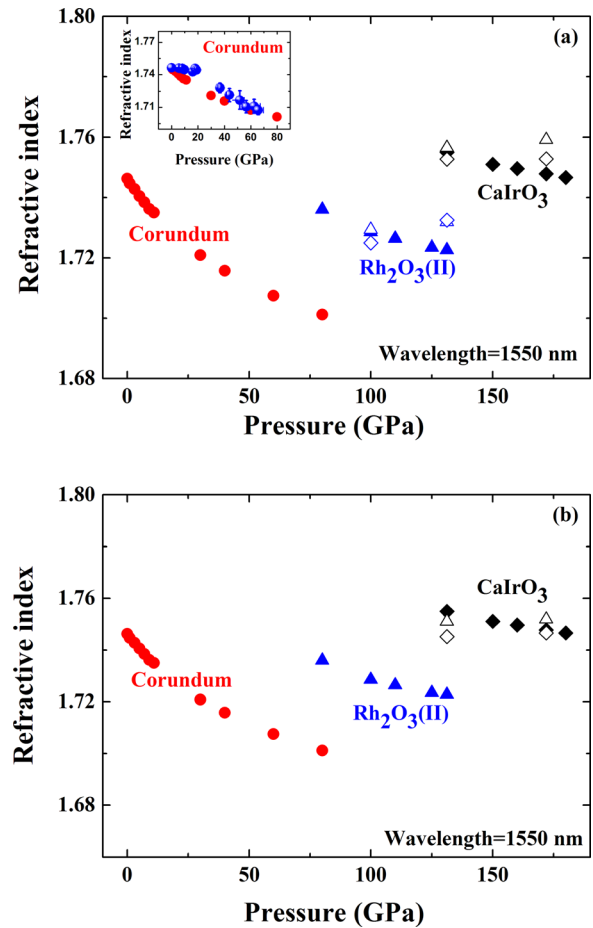


FIG. 6. Calculated refractive-index data vs. pressure. The solid spheres, circles, triangles, and diamonds denote the experimental data, the calculated refractive index of perfect corundum, Rh_2O_3 (II), and CaIrO_3 phase regions, respectively. The open triangles and diamonds denote the calculated refractive index of the crystals with Al or O vacancy defects, respectively. (a) The Al or O vacancy-defect concentrations adopted in the calculations were 1.25% at 100 GPa, 1.67% at 131.2 GPa, and 2.5% at 172 GPa, respectively. (b) The Al or O vacancy-defect concentrations adopted in the CaIrO_3 phase were 1.25% at 131.2 GPa and 1.67% at 172 GPa, respectively.

vacancy defects in sapphire are mostly stable in their fully ionized state.³⁸ Hence, we only investigated the influences of the -3 charged Al and $+2$ charged O vacancies on the high-pressure refractive index of Al_2O_3 (more details are shown in the [supplementary material](#)). The calculated results show that the vacancy-defect factor influences the pressure-change tendencies of the refractive index in the Rh_2O_3 (II) and CaIrO_3 phase regions [Fig. 6(a)]: noticeably weakening the decreasing trend of the refractive index with pressure in the Rh_2O_3 (II) phase region and increasing the refractive index in the CaIrO_3 phase region with increasing pressure. Moreover, data calculated with relatively lower vacancy-defect concentration models at two pressure points of the CaIrO_3 phase region also support these results [Fig. 6(b)]. In addition, the pressure-change tendencies of the calculated refractive-index data in the corundum-phase region agreed with the pressure-change tendency of the first segment of the experimental points. This should stem from the weak influences of the temperature and defect factors because shock-temperature and shock-induced vacancy-defect concentration are low under weak shock compression and have negligible effects on the

refractive index of shocked Al_2O_3 . This idea may also explain the analogous phenomenon appearing in LiF .³⁷ Finally, note that the pressure points of the refractive-index discontinuously change in the calculations were different from those observed in our shock experiments. This is because for our first-principles calculations the structural-transition pressure points were based on the static high-pressure results in Ref. 16. However, these differences did not influence our analysis of the shock experimental data.

Besides vacancy defects, strong shock compression could induce line-, planar- and body-defects in a sapphire crystal.³⁹ These defects might also affect its high-pressure refractive index. But, due to calculation limitations, it is difficult for us to estimate their contributions. Even so, we still think that they could reasonably explain the differences between our experimental and calculated results in terms of the shock-induced temperature and vacancy-defect effects. Therefore, we deduce that the two discontinuities phenomena observed in our Al_2O_3 refractive index measurements arose from the shock-induced corundum- $\text{Rh}_2\text{O}_3(\text{II})$ and $\text{Rh}_2\text{O}_3(\text{II})$ - CaIrO_3 structural transitions. Our study indicates that although high-pressure structural transitions in Al_2O_3 are difficult to detect via Hugoniot measurements, they may be observed clearly by shock refractive-index experiments. This provides some useful guidance for shock-transition investigations of transparent materials in the future.

IV. CONCLUSION

Plate impact experiments were performed on a sapphire single crystal to measure its optical refractive index under shock pressure up to 210 GPa. We observed two discontinuities in the refractive index at ~ 65 to 92 GPa and ~ 144 to 163 GPa, respectively. The pressure dependence of the sapphire refractive index above the HEL was divided into three segments, and their pressure-change trends were completely different. The refractive index decreased noticeably with pressure in the first segment (~ 20 to 65 GPa), remained almost constant from 92 GPa to 144 GPa in the second segment, and evidently increased with pressure in the third segment (~ 163 to 210 GPa). According to our analytical results from the phase diagram and first-principles calculations, we judge that the two discontinuities in the refractive index arose from the shock-induced corundum- $\text{Rh}_2\text{O}_3(\text{II})$ and $\text{Rh}_2\text{O}_3(\text{II})$ - CaIrO_3 structural transitions in sapphire. The existence of high-concentration vacancy defects under strong shock compression had a significant influence on the refractive-index change behaviors of the sapphire high-pressure phases. This may be the origin of the great discrepancies in the pressure-change trends of the three segments observed in our experiments. Our results suggest that: (1) information about the sapphire refractive index under strong shock compression cannot be obtained by the simple extrapolation of its low-pressure data, implying that the refractive-index measurements within a wide shock-pressure range are vital for laser interferometer experiments. (2) Shock-induced phase transitions may exist in sapphire below 200 GPa. (3) The refractive-index measurement of transparent materials

under shock loading should be a feasible approach to explore its phase transitions.

SUPPLEMENTARY MATERIAL

See [supplementary material](#) for the theoretical calculation details.

ACKNOWLEDGMENTS

We gratefully acknowledge Professor Hongliang He, from the Institute of Fluid Physics, for his valuable discussions during the preparation of this manuscript, and are grateful to Professor Xianming Zhou of the Peac Institute of Multiscale Sciences for his useful suggestions for our experimental measurements. This work was financially supported by the National Natural Science Foundation of China under Grant Nos. 11602244 and 11602245.

- ¹N. C. Holmes, M. Ross, and W. J. Nellis, *Phys. Rev. B* **52**, 15835 (1995).
- ²J. L. Pélissier and D. Partouche-Sebban, *Phys. B* **364**, 14 (2005).
- ³Y. M. Gupta, P. D. Horn, and J. A. Burt, *J. Appl. Phys.* **76**, 1784 (1994).
- ⁴L. M. Barker and R. E. Hollenbach, *J. Appl. Phys.* **41**, 4208 (1970).
- ⁵Y. S. Xu, C. McCammon, and B. T. Poe, *Science* **282**, 922 (1998).
- ⁶A. R. Oganov and S. Ono, *Proc. Natl. Acad. Sci. U. S. A.* **102**, 10828 (2005).
- ⁷R. E. Setchell, *J. Appl. Phys.* **50**, 8186 (1979).
- ⁸R. E. Setchell, *J. Appl. Phys.* **91**, 2833 (2002).
- ⁹S. C. Jones, M. C. Robinson, and Y. M. Gupta, *J. Appl. Phys.* **93**, 1023 (2003).
- ¹⁰S. C. Jones, B. A. M. Vaughan, and Y. M. Gupta, *J. Appl. Phys.* **90**, 4990 (2001).
- ¹¹B. J. Jensen, D. B. Holtkamp, and P. A. Rigg, *J. Appl. Phys.* **101**, 013523 (2007).
- ¹²X. X. Cao, J. B. Li, J. Li, X. H. Li, L. Xu, Y. Wang, W. J. Zhu, C. H. Meng, and X. M. Zhou, *J. Appl. Phys.* **116**, 093516 (2014).
- ¹³X. M. Li, Y. Y. Yu, Y. H. Li, L. Zhang, and J. D. Weng, *J. Appl. Phys.* **109**, 103518 (2011).
- ¹⁴J. D. Weng, H. Tan, X. Wang, Y. Ma, S. L. Hu, and X. S. Wang, *Appl. Phys. Lett.* **89**, 111101 (2006).
- ¹⁵J. F. Lin, O. Degtyareva, C. T. Prewitt, P. Dera, N. Sata, E. Gregoryanz, H. K. Mao, and R. J. Hemley, *Nat. Mater.* **3**, 389 (2004).
- ¹⁶S. Ono, A. R. Oganov, T. Koyama, and H. Shimizu, *Earth Planet. Sci. Lett.* **246**, 326 (2006).
- ¹⁷J. Kato, K. Hirose, H. Ozawa, and Y. Ohishi, *Am. Miner.* **98**, 335 (2013).
- ¹⁸R. G. McQueen and S. P. Marsh, *Handbook of Physical Constants* (The Geological Society of America, New York, 1966), p. 154.
- ¹⁹S. P. Marsh, in *LASL Shock Hugoniot Data* (University of California Press, Berkeley, 1980), p. 260.
- ²⁰D. Erskine, in *High-Pressure Science and Technology Part I*, edited by S. C. Schmidt, J. W. Shaner, G. A. Samara, and M. Ross (American Institute of Physics, New York, 1994), p. 141.
- ²¹R. A. Graham and W. P. Brooks, *J. Phys. Chem. Solids* **32**, 2311 (1971).
- ²²S. T. Weir, A. C. Mitchell, and W. J. Nellis, *J. Appl. Phys.* **80**, 1522 (1996).
- ²³S. T. Weir, A. C. Mitchell, and W. J. Nellis, *Phys. Rev. Lett.* **76**, 1860 (1996).
- ²⁴L. He, M. J. Tang, Y. Fang, and F. Q. Jing, *Europhys. Lett.* **83**, 39001 (2008).
- ²⁵A. Dewaele, J. Eggert, P. Loubeyre, and R. LeToullec, *Phys. Rev. B* **67**, 094112 (2003).
- ²⁶J. W. Huang, Q. C. Liu, X. L. Zeng, X. M. Zhou, and S. N. Luo, *J. Appl. Phys.* **118**, 205902 (2015).
- ²⁷D. Hayes, *J. Appl. Phys.* **89**, 6484 (2001).
- ²⁸D. E. Fratanduono, J. H. Eggert, M. C. Akin, R. Chau, and N. C. Holmes, *J. Appl. Phys.* **114**, 043518 (2013).
- ²⁹S. P. Marsh, *LASL Shock Hugoniot data* (University of California Press, Berkeley, 1980), pp. 57–212.
- ³⁰F. Xi, K. Jin, L. C. Cai, H. Y. Geng, Y. Tan, and J. Li, *J. Appl. Phys.* **117**, 185901 (2015).

- ³¹P. A. Urtiew, *J. Appl. Phys.* **45**, 3490 (1974).
- ³²D. E. Hare, D. J. Webb, S. H. Lee, and H. C. Homes, in *Shock Compression of Condensed Matter-2001*, edited by M. D. Furnish, N. N. Thadhani, and Y. Horie (American Institute of Physics, New York, 2002), p. 1231.
- ³³J. L. Wise and L. C. Chhabildas, in *Shock Waves in Condensed Matter*, edited by Y. M. Gupta (Springer, Boston, MA, USA, 1986), pp. 441–454.
- ³⁴F. Q. Jing, *Introduction to Experimental Equation of State* (Science, Beijing, 1999), pp. 60–66.
- ³⁵E. R. Dobrovinskaya *et al.*, *Sapphire: Material, Manufacturing, Applications* (Springer, 1970), p. 55.
- ³⁶M. A. Meyers, *Dynamic Behavior of Materials* (Wiley-IEEE, New York, 1994), pp. 413–415.
- ³⁷L. He, M. J. Tang, J. Yin, X. M. Zhou, W. J. Zhu, F. S. Liu, and D. W. He, *Phys. B* **407**, 694 (2012).
- ³⁸K. Matsunaga, T. Tanaka, T. Yamamoto, and Y. Ikuhara, *Phys. Rev. B* **68**, 085110 (2003).
- ³⁹Y. Wang and D. E. Mikkola, *Mater. Sci. Eng. A* **148**, 25 (1991).